

Article

# Generalized One-Dimensional Periodic Potential Wells Tending to the Dirac Delta Potential

F. Mendoza-Villa <sup>1</sup>, Juan A. Ramos-Guivar <sup>1</sup> and R. M. Espinoza-Bernardo <sup>2,\*</sup>

<sup>1</sup> Grupo de Investigación de Nanotecnología Aplicada para Biorremediación Ambiental, Energía, Biomedicina y Agricultura (NANOTECH), Facultad de Ciencias Físicas, Universidad Nacional Mayor de San Marcos, Av. Venezuela Cdra 34 S/N, Ciudad Universitaria, Lima 15081, Peru; freddy.mendoza1@unmsm.edu.pe (F.M.-V.); juan.ramos5@unmsm.edu.pe (J.A.R.-G.)

<sup>2</sup> Grupo de Métodos Computacionales Aplicado a Nanomateriales (GMCAN), Facultad de Ciencias Físicas, Universidad Nacional Mayor de San Marcos, P.O. Box 14-0149, Lima 15081, Peru;

\* Correspondence: robert.espinoza2@unmsm.edu.pe

**Abstract:** The solution of a quantum periodic potential in solid state physics is relevant because one can understand how electrons behave in a corresponding crystal. In this paper, the analytical solution of the energy formulation for a one-dimensional periodic potential that meets certain boundary conditions is developed in a didactic and detailed way. In turn, the group speed and effective mass are also calculated from the transcendental energy equation of a potential  $V = V(x)$ . From this, a comparison is made with periodic potentials with known analytical solutions, such as the Dirac delta, as well as rectangular and triangular potentials. Finally, some limits are proposed in which these periodic potentials of the form  $V = V(x)$  approach the periodic Dirac delta potential of positive intensity. Therefore, the calculations described in this paper can be used as the basis for more-complex one-dimensional potentials and related simulations.

**Keywords:** Dirac delta potential; one-dimensional periodic potential; computational physics; rectangular potential; triangular potential; asymmetric potential



**Citation:** Mendoza-Villa, F.; Ramos-Guivar, J.A.; Espinoza-Bernardo, R.M. Generalized One-Dimensional Periodic Potential Wells Tending to the Dirac Delta Potential. *Physics* **2024**, *6*, 75–93. <https://doi.org/10.3390/physics6010006>

Received: 10 October 2023

Revised: 23 November 2023

Accepted: 2 December 2023

Published: 9 January 2024



**Copyright:** © 2024 by the authors. Licensee MDPI, Basel, Switzerland. This article is an open access article distributed under the terms and conditions of the Creative Commons Attribution (CC BY) license (<https://creativecommons.org/licenses/by/4.0/>).

## 1. Introduction

The study of periodic potentials is highly important in condensed matter physics. Band structure engineering has its basis in Bloch's theorem [1] and represents a daily quantum mechanical problem, which can be solved by two known methods [2]: the transfer matrix method, which is valid for all types of periodic potentials, and the variational method, in which weak potentials allow for the approximation of potentials of different corresponding geometries [3–6].

The solutions of periodic potentials have been worked out by many authors, but without using Bloch's theorem [7–14]. The Kronig–Penney model is one of the periodic potentials that has received the most attention because it provides a solution to the Schrödinger equation (SE) that is independent of time and represented by a set of wave plane functions. It is possible to solve the SE by using its transcendental energy equation [4,15]. This example is the most known for explaining energy bands and is the easiest for calculating the limits that approach the Dirac delta potential [5]. This calculation can be performed for a periodic potential with a finite or infinite range of intensities, both positively and negatively [16,17]. Nevertheless, only positive intensity cases are considered in this study.

In addition, among the potential wells, the most known one is the rectangular well followed by the triangular well. The solution functions of this potential have been previously evaluated [18]. This potential is applied in uniform fields such as the gravitational field in neutrons [19,20], the triangular potential plus the infinite potential barrier to find the transmission and reflection coefficients, and the electrical conduction through thin

polyvinyl butyral (PVB) films. PVB is a polymer that is used in the manufacture of laminated glass [20–22]. Previous studies of the periodic triangular potential have resolved problems of this kind, but without connecting the matching null potential [3,4].

The aim of this study is to obtain analytical equations for the transcendental equation of energy and the corresponding group speed and effective mass for the studied one-dimensional potential wells, which have a solution to the SE. To do that, we generalize the results of the Kronig–Penney potential with respect to the band theory to various one-dimensional potentials [5,15]. Here, we propose a general solution for a group of one-dimensional potential wells that, upon approximation, tends to a Dirac delta potential of positive intensity [17,23,24]. From this general equation, the transcendental energy equation is solved by a detailed mathematical demonstration; the group speed and the corresponding effective mass are calculated as a function of the wave number, representing solutions to the SE for a potential of  $V = V(x)$  [24,25]. To verify the results, the approximation is carried out when the barriers are infinitely large and thin, that is the width,  $b$ , of the potential tends to zero and the height,  $w$ , of the potential tends to infinity [17,23,24].

### 2. Theoretical Model and Simulation Details

To find the general solution of an even function whose periodic potential is of the form  $V = V(x)$ , first, the global minima must be satisfied, which are located at the edges of the interval  $x = \pm b$ , with the global maxima located at  $x = 0$ :

$$V(x) = \begin{cases} V(\pm b) & = 0, \\ V(0) & = w, \end{cases} \tag{1}$$

where  $w$  is the height of the potential  $V(x)$ ,  $a$  is the separation between the potentials ( $V(x)$ ),  $b$  is the width of the potential  $V(x)$ , and  $T = 2b + a$  is the period of the periodic potential.

Figure 1 represents the quantum potentials studied in this paper, which meet the conditions given in Equation (1). Some potentials are known to have an analytic solution. Examples include the positive-intensity Dirac delta potential, whose solution is a linear combination of complex exponentials, and the rectangular potential, whose solution is a linear combination of real exponentials. However, other types of potentials either lack analytic solutions or depend on special functions. Therefore, the theory of perturbations (small potentials) or numerical analysis (Ritz method) is used, known as the Rayleigh–Ritz method, which is commonly used in quantum mechanics to solve the SE [26].

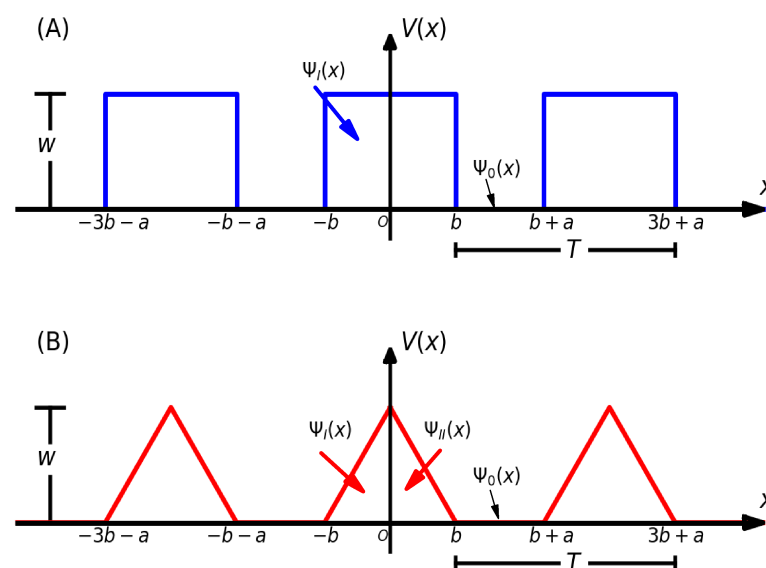


**Figure 1.** Representation of the periodic potential studied in this paper. (A) For a potential  $V(x)$ , and a zero potential. (B) For two potentials,  $V_1(x)$ ,  $V_2(x)$ , and a zero potential. Both potentials have the same period  $T = 2b + a$  and the same height  $w$ .

To address this problem, we assumed that the SE for a potential of  $V = V(x)$  meets the above conditions and has exact solutions ( $y_1(x), y_2(x), z_1(x)$  and  $z_2(x)$ ) in the range of  $x \in [-b, b]$ , while their corresponding derivatives are represented by ( $y'_1(x), y'_2(x), z'_1(x)$  and  $z'_2(x)$ ). With the aim of discussing the approximation of a periodic potential  $V = V(x)$  of Dirac delta potential, the ideas proposed by Bloch are used. According to Bloch's theorem, the periodic wave function,  $\Psi(x)$ , is equal to the product of a periodic function ( $u(x)$ ) and a plane wave ( $e^{ikx}$ ). This function is known as the Bloch wave because it has the formula  $\Psi(x) = e^{ikx}u(x)$ :

- The boundary conditions and continuity of the wave functions  $\Psi_I(x)$  and  $\Psi_0(x)$  for the potential of Figure 1A:

$$\Psi_I(b) = \Psi_0(b), \tag{2}$$

$$\Psi_I(-b) = e^{ikT}\Psi_0(b+a), \tag{3}$$

$$\Psi'_I(b) = \Psi'_0(b), \tag{4}$$

$$\Psi'_I(-b) = e^{ikT}\Psi'_0(b+a). \tag{5}$$

Equations (2)–(5) represent the boundary and continuity conditions for the case of a potential of  $V = V(x)$  and a zero potential.

- The boundary conditions and continuity of the wave functions  $\Psi_I(x), \Psi_{II}(x)$  and  $\Psi_0(x)$  for the potential of Figure 1B:

$$\Psi_I(0) = \Psi_{II}(0), \tag{6}$$

$$\Psi'_I(0) = \Psi'_{II}(0), \tag{7}$$

$$\Psi_{II}(b) = \Psi_0(b), \tag{8}$$

$$\Psi'_{II}(b) = \Psi'_0(b), \tag{9}$$

$$\Psi_I(-b) = e^{ikT}\Psi_0(b+a), \tag{10}$$

$$\Psi'_I(-b) = e^{ikT}\Psi'_0(b+a). \tag{11}$$

Equations (6)–(11) represent the boundary and continuity conditions for the case of two potentials of  $V = V(x)$  and zero potential. The transcendental energy equation for the Dirac delta potential of positive intensity is given by the following equation [17,23,27]:

$$\cos(ka) = \frac{P}{\alpha a} \sin(\alpha a) + \cos(\alpha a), \tag{12}$$

where  $a$  is the period of Equation (12),  $P$  is a finite quantity, and the variable  $\alpha$  is a function of energy in Equation (12).  $\alpha$  is expressed as  $\sqrt{2mE}/\hbar$ , where  $m$  and  $E$  denote the mass and the energy of a particle and  $\hbar$  is the reduced Planck's constant. Figure 2 shows the energy for the Dirac delta periodic potential as a function of the wave number. This is the graph that the other periodic potentials of different geometries must approximate when the width  $b$  is infinitely small and the height  $w$  is infinitely large.

### 2.1. Periodic Potential of One Potential $V = V(x)$ and a Zero Potential

The form of the potential  $V = V(x)$  studied in this Section is given by the equation,

$$V(x) = \begin{cases} V_1(x) & \wedge \quad -b < x < b, \\ 0 & \wedge \quad b < x < b+a, \end{cases} \tag{13}$$

where  $V_1(x)$  is a potential of Equation (13) that satisfies the conditions of Equation (1).

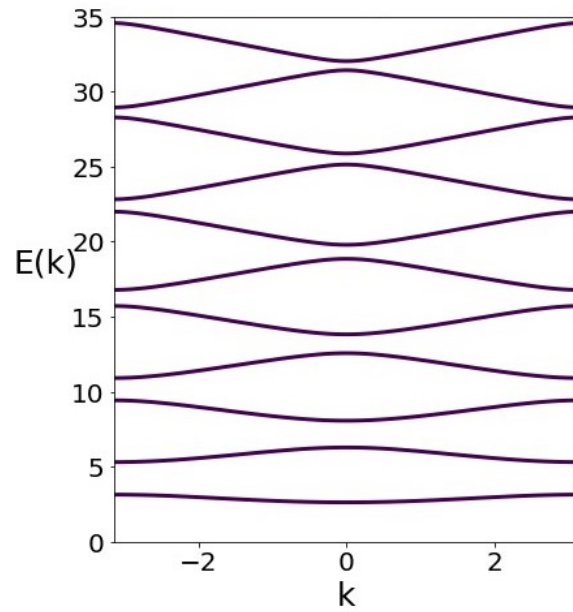


Figure 2. Graph of the transcendental energy equation for the Dirac delta potential (12) using  $P = 10$ .

The wave function  $\Psi_I(x)$  is the potential solution for  $V_1(x)$  in this specific case. Using Bloch’s theory, one can derive the following transcendental energy equation from the secular determinant,

$$0 = \begin{vmatrix} y_1(b) & y_2(b) & -e^{i\alpha b} & -e^{-i\alpha b} \\ y_1(-b) & y_2(-b) & -e^{ikT} e^{i\alpha(b+a)} & -e^{ikT} e^{-i\alpha(b+a)} \\ y_1'(b) & y_2'(b) & -i\alpha e^{i\alpha b} & i\alpha e^{-i\alpha b} \\ y_1'(-b) & y_2'(-b) & -i\alpha e^{ikT} e^{i\alpha(b+a)} & i\alpha e^{ikT} e^{-i\alpha(b+a)} \end{vmatrix}, \tag{14}$$

where  $y_1(x), y_2(x)$  are solutions of the SE for the potential  $V = V_1(x)$ . Now, solving the determinant of Equation (14), one obtains the following solution expressed by the equation,

$$\cos(k(2b + a)) = \frac{\sin(\alpha a)}{\alpha} \left[ \frac{M_1(E) + \alpha^2 M_2(E)}{M_4(E)} \right] + \cos(\alpha a) \left[ \frac{M_3(E)}{M_4(E)} \right]. \tag{15}$$

The form of Equation (15) matches the Dirac delta potential and the rectangular potential’s transcendental energy equation. The derivation of Equation (15) can be revised in Section 1 of the Supplementary Materials to this paper. The variables  $M_1(E), M_2(E), M_3(E)$ , and  $M_4(E)$  are functions of the energy, and they are given by the following equations:

$$M_1(E) = y_2'(-b)y_1'(b) - y_2'(b)y_1'(-b), \tag{16}$$

$$M_2(E) = y_2(-b)y_1(b) - y_2(b)y_1(-b), \tag{17}$$

$$M_3(E) = y_1(b)y_2'(-b) - y_1'(-b)y_2(b) + y_1(-b)y_2'(b) - y_1'(b)y_2(-b), \tag{18}$$

$$M_4(E) = 2W\{y_1(x), y_2(x)\}. \tag{19}$$

$W\{y_1(x), y_2(x)\}$  represents the Wronskian of the wave functions for the potential  $V_1(x)$ . The energy variables  $M_1(E), M_2(E), M_3(E)$ , and  $M_4(E)$  (16)–(19) must satisfy the following limits:

$$\lim_{(b,w) \rightarrow (0,\infty)} \left[ \frac{M_1(E) + \alpha^2 M_2(E)}{M_4(E)} \right] = F(b, w), \tag{20}$$

$$\lim_{(b,w) \rightarrow (0,\infty)} \left[ \frac{M_3(E)}{M_4(E)} \right] = 1. \tag{21}$$

Since we want to approximate the potential  $V = V(x)$  to the Dirac delta potential, they must satisfy Equations (20) and (21).  $F(b, w)$  is a function that depends on  $b$  and  $w$ .

2.2. Periodic Potential of Two Potentials  $V = V(x)$  and a Zero Potential

The form of the potential  $V = V(x)$  under study in this Section is given by the following equation:

$$V(x) = \begin{cases} V_1(x) & \wedge & -b < x < 0, \\ V_2(x) & \wedge & 0 < x < b, \\ 0 & \wedge & b < x < b + a, \end{cases} \tag{22}$$

where  $V_1(x)$  and  $V_2(x)$  are potentials of Equation (22) that satisfy the conditions of Equation (1).

The periodic potential involves three potentials  $V_1(x)$ ,  $V_2(x)$ , and  $V_3(x)$ , where the potential  $V_3(x)$  is the zero potential and the potentials  $V_1(x)$  and  $V_2(x)$  that fulfill that the global minimum must be  $x = \pm b$  and the global maximum at  $x = 0$ . Now, using Bloch’s theorem, one obtains the following secular determinant:

$$0 = \begin{vmatrix} y_1(0) & y_2(0) & -z_1(0) & -z_2(0) & 0 & 0 \\ 0 & 0 & z_1(b) & z_2(b) & -e^{i\alpha b} & -e^{-i\alpha b} \\ y_1(-b) & y_2(-b) & 0 & 0 & -e^{ikT}e^{i\alpha(b+a)} & -e^{ikT}e^{-i\alpha(b+a)} \\ y_1'(0) & y_2'(0) & -z_1'(0) & -z_2'(0) & 0 & 0 \\ 0 & 0 & z_1'(b) & z_2'(b) & -i\alpha e^{i\alpha b} & i\alpha e^{-i\alpha b} \\ y_1'(-b) & y_2'(-b) & 0 & 0 & -i\alpha e^{ikT}e^{i\alpha(b+a)} & i\alpha e^{ikT}e^{-i\alpha(b+a)} \end{vmatrix}, \tag{23}$$

where  $y_1(x)$ ,  $y_2(x)$  are the solutions of the SE for the potential  $V = V_1(x)$  and  $z_1(x)$ ,  $z_2(x)$  are the solutions of the SE for the potential  $V = V_2(x)$ . The secular determinant (23) has a solution

$$\cos(k(2b + a)) = \frac{\sin(\alpha a)}{\alpha} \left[ \frac{N_1(E) + \alpha^2 N_2(E)}{N_4(E)} \right] + \cos(\alpha a) \left[ \frac{N_3(E)}{N_4(E)} \right]. \tag{24}$$

Equation (24) has the same form as Equation (16), with the only difference being the energy variables  $N_1(E)$ ,  $N_2(E)$ ,  $N_3(E)$ , and  $N_4(E)$ :

$$N_1(E) = [y_1(0)y_2'(-b) - y_2(0)y_1'(-b)] \cdot [z_2'(0)z_1'(b) - z_1'(0)z_2'(b)] + [z_2(0)z_1'(b) - z_1(0)z_2'(b)] \cdot [y_1'(-b)y_2'(0) - y_2'(-b)y_1'(0)], \tag{25}$$

$$N_2(E) = [y_1(0)y_2(-b) - y_2(0)y_1(-b)] \cdot [z_2(b)z_1'(0) - z_1(b)z_2'(0)] + [z_2(0)z_1(b) - z_1(0)z_2(b)] \cdot [y_2(-b)y_1'(0) - y_1(-b)y_2'(0)], \tag{26}$$

$$N_3(E) = [y_2(0)y_1(-b) - y_1(0)y_2(-b)] \cdot [z_2'(0)z_1'(b) - z_1'(0)z_2'(b)] + [z_2(0)z_1'(b) - z_1(0)z_2'(b)] \cdot [y_2(-b)y_1'(0) - y_1(-b)y_2'(0)] + [y_1(0)y_2'(-b) - y_2(0)y_1'(-b)] \cdot [z_1(b)z_2'(0) - z_2(b)z_1'(0)] + [z_1(0)z_2(b) - z_2(0)z_1(b)] \cdot [y_2'(-b)y_1'(0) - y_1'(-b)y_2'(0)], \tag{27}$$

$$N_4(E) = 2W\{y_1(x), y_2(x)\} \cdot W\{z_1(x), z_2(x)\}, \tag{28}$$

where the energy variables  $N_1(E)$ ,  $N_2(E)$ ,  $N_3(E)$ , and  $N_4(E)$  (25)–(28) of Equation (24) are different energy functions (16)–(19) of Equation (15). The deduction of Equation (24) is given in Section S2 of the Supplementary Materials of this paper.

$W\{y_1(x), y_2(x)\}$  and  $W\{z_1(x), z_2(x)\}$  represents the Wronskian of the wave functions for the potentials  $V_1(x)$  and  $V_2(x)$ . The energy variables  $N_1(E), N_2(E), N_3(E)$ , and  $N_4(E)$  (25)–(28) must satisfy the following limits:

$$\lim_{(b,w) \rightarrow (0,\infty)} \left[ \frac{N_1(E) + \alpha^2 N_2(E)}{N_4(E)} \right] = G(b, w), \tag{29}$$

$$\lim_{(b,w) \rightarrow (0,\infty)} \left[ \frac{N_3(E)}{N_4(E)} \right] = 1. \tag{30}$$

Since we want to approximate the potential  $V = V(x)$  to the Dirac delta potential, the latter must satisfy Equations (29) and (30) the same for the case of a potential  $V = V(x)$  with zero potential. Again,  $G(b, w)$  is a function that depends on  $b$  and  $w$  only.

### 2.3. The Group Speed

The transcendental energy equation is known for any potential  $V = V(x)$  that meets the aforementioned conditions and that has the form of a periodic potential, or a potential  $V = V(x)$  plus a zero or two potentials of the type  $V = V(x)$  together with a zero potential, which are given by Equations (15) and (24). The latter potentials can be rewritten as energy functions to facilitate the calculation of the group speed and effective mass, following the equation

$$\cos(kT) = f(E) \sin(\alpha(E)a) + g(E) \cos(\alpha(E)a), \tag{31}$$

where the energy functions  $f(E)$  and  $g(E)$  are the grouping of the energy variables  $M_1(E), M_2(E), M_3(E)$ , and  $M_4(E)$  of Equation (15) or  $N_1(E), N_2(E), N_3(E)$ , and  $N_4(E)$  of Equation (24). Additionally,  $f(E)$  and  $g(E)$  are shown as a function of  $y_1(x), y_2(x), z_1(x)$ , and  $z_2(x)$  in Section S3 of the Supplementary Materials to this paper:

$$f(E) = \frac{M_1(E) + \alpha^2 M_2(E)}{\alpha M_4(E)}, \quad f(E) = \frac{N_1(E) + \alpha^2 N_2(E)}{\alpha N_4(E)}, \tag{32}$$

$$g(E) = \frac{M_3(E)}{M_4(E)}, \quad g(E) = \frac{N_3(E)}{N_4(E)}, \tag{33}$$

Therefore, the corresponding group speed can be calculated based on Equations (32) and (33), which is directly proportional to the derivative of the energy  $E$  with respect to the wave number  $k$  [24,25]:

$$v_G = \frac{1}{\hbar} \frac{dE}{dk}. \tag{34}$$

The form of the group speed is obtained by calculating the derivative of the energy with respect to the wave number divided by the Dirac constant found in Equation (34):

$$v_G = \frac{T \sin(kT)}{\hbar H_0(E)}. \tag{35}$$

where  $T = 2b + a$  is the period of the periodic potential. On the other hand, the energy function  $H_0(E)$  has the following form as a function of the energy variables  $f(E)$  and  $g(E)$ :

$$H_0(E) = \left( ag(E) \frac{d\alpha(E)}{dE} - \frac{df(E)}{dE} \right) \sin(\alpha(E)a) - \left( af(E) \frac{d\alpha(E)}{dE} + \frac{dg(E)}{dE} \right) \cos(\alpha(E)a). \tag{36}$$

The energy variable  $H_0(E)$  (36) is also derived in Section S4 of the Supplementary Material of this paper. From Equation (35) of the group speed, one can deduce using the first derivative criterion that, for the values of the wave number  $k = [0, \pi/T]$ , the group speed is equal to zero, that is actually, no energy is transported [28]. This is because the group speed lies at the limit between the energy values of the allowed and the forbidden energy

bands of the periodic potential, since, by replacing  $k = [0, \pi/T]$  in the transcendental energy equation, those corresponding limits are

$$-1 \leq f(E) \sin(\alpha a) + g(E) \cos(\alpha a) \leq 1. \tag{37}$$

The inequality (37) describes the bounds that the transcendental energy equation of the periodic potential of Equations (15) and (24) must have.

#### 2.4. The Effective Mass

Like the group speed, the effective mass can also be calculated as

$$\frac{1}{m^*} = \frac{1}{\hbar^2} \frac{d^2 E}{dk^2}. \tag{38}$$

The form of the effective mass (38) is obtained by calculating the inverse of the second derivative of the energy with respect to the wave number multiplied by the square of the Dirac constant. The calculations give:

$$m^* = \frac{\hbar^2 H_2(E)}{T^2 \cos(kT) - \hbar^2 v_G^2 H_1(E)}, \tag{39}$$

where, from Equation (39),  $T = 2b + a$  is the period of the periodic potential. The functions  $H_1(E)$  and  $H_2(E)$  have the following form:

$$\begin{aligned} H_1(E) = & \left[ ag(E) \frac{d^2 \alpha(E)}{dE^2} + 2a \frac{dg(E)}{dE} \frac{d\alpha(E)}{dE} \right] \sin(\alpha(E)a) \\ & - \left[ \frac{d^2 f(E)}{dE^2} - a^2 f(E) \left( \frac{d\alpha(E)}{dE} \right)^2 \right] \sin(\alpha(E)a) \\ & - \left[ af(E) \frac{d^2 \alpha(E)}{dE^2} + 2a \frac{df(E)}{dE} \frac{d\alpha(E)}{dE} \right] \cos(\alpha(E)a) \\ & - \left[ \frac{d^2 g(E)}{dE^2} - a^2 g(E) \left( \frac{d\alpha(E)}{dE} \right)^2 \right] \cos(\alpha(E)a), \end{aligned} \tag{40}$$

$$H_2(E) = \left( ag(E) \frac{d\alpha(E)}{dE} - \frac{df(E)}{dE} \right) \sin(\alpha(E)a) - \left( af(E) \frac{d\alpha(E)}{dE} + \frac{dg(E)}{dE} \right) \cos(\alpha(E)a), \tag{41}$$

as functions of the variables  $f(E)$  and  $g(E)$ . Finally,  $v_G$  is the group speed of the periodic potential.

Additionally, the energy variables  $H_1(E)$  and  $H_2(E)$  in Equations (40) and (41) are obtained in Section S5 of the Supplementary Materials of this paper. From the effective mass equation (39), it can also be deduced that there is a discontinuity at a point of wave number  $k$ . The wave number  $k$  is the solution of the following transcendental equation:

$$\cos(kT) = \frac{1}{H_1(E)} \left( \frac{\hbar v_G}{T} \right)^2. \tag{42}$$

Finally, the value of  $k$  obtained from Equation (42) represents the existence of an inflection point, that is the change in the concavity of the transcendental energy equation in the domain of the wave number.

### 3. Results

#### 3.1. Periodic Potential of One Potential $V = V(x)$ and a Zero Potential

The energy functions  $M_1(E), M_2(E), M_3(E)$ , and  $M_4(E)$  obtained from Equation (15) were calculated for the rectangular potential  $V_1(x) = w$ , which are found in terms of hyperbolic functions and of  $\beta = \sqrt{2m(w - E)}/\hbar$ :

$$M_1(E) = -2\beta^2 \sinh(2\beta b), \tag{43}$$

$$M_2(E) = 2 \sinh(2\beta b), \tag{44}$$

$$M_3(E) = -4\beta \cosh(2\beta b), \tag{45}$$

$$M_4(E) = -4\beta. \tag{46}$$

The energy functions  $M_1(E), M_2(E), M_3(E)$ , and  $M_4(E)$  (16)–(19) are replaced in the transcendental energy equation, and the following equation is obtained:

$$\cos(k(2b + a)) = \frac{(\beta^2 - a^2)}{2\beta a} \sinh(2\beta b) \sin(\alpha a) + \cosh(2\beta b) \cos(\alpha a). \tag{47}$$

Figure 3 shows the curve for the equation of the transcendental energy of the rectangular potential; this curve is similar to the Dirac delta potential energy, since the value of the width  $2b$  and the height  $w$  proposed are those indicated to carry out this approach.

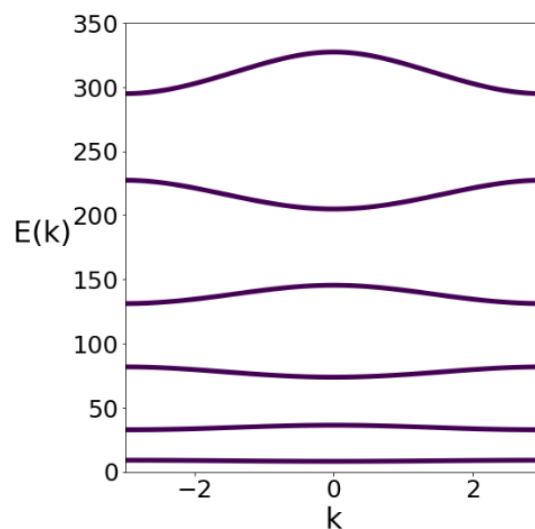


**Figure 3.** Graph of the transcendental energy equation of the rectangular potential (47) for  $w = 1000$ ,  $b = 0.025$ ,  $a = 1$ , and the area  $A = 2bw = 50$ .

The transcendental energy equation for the rectangular potential well  $V(x) = w$  is the one obtained by solving the secular determinant of Equation (14), obtaining Equation (47) as a solution. Therefore, the transcendental energy equation satisfies the Kronig–Penney model.

Furthermore, it is demonstrated that, by employing Equation (24), one may obtain the same transcendental energy equation that fulfills the Kronig–Penney model. This implies that particular cases of Equation (24) can approach Equation (15). As a result, the calculations made when solving Equations (15) and (24) are correct.

#### 3.2. Periodic Potential of Two Potentials $V = V(x)$ and a Zero Potential

The energy functions  $N_1(E), N_2(E), N_3(E)$ , and  $N_4(E)$  were calculated from Equation (24) for the rectangular potential  $V_1(x) = (w/b)(x + b)$  and  $V_2(x) = (w/b)(b - x)$ , which are in terms of Airy special functions [22,29]. However, the computation of the energy functions  $N_1(E), N_2(E), N_3(E)$ , and  $N_4(E)$  is quite lengthy so not given here. As so, in Section S2 of the Supplementary Material of this paper, the wave functions  $y_1(x), y_2(x), z_1(x)$ , and

$z_2(x)$  that compose the transcendental energy equation are presented, corresponding to the special Airy functions.

The numerical simulation of the transcendental energy equation for the triangular potential is shown in Figure 4 for certain corresponding values.

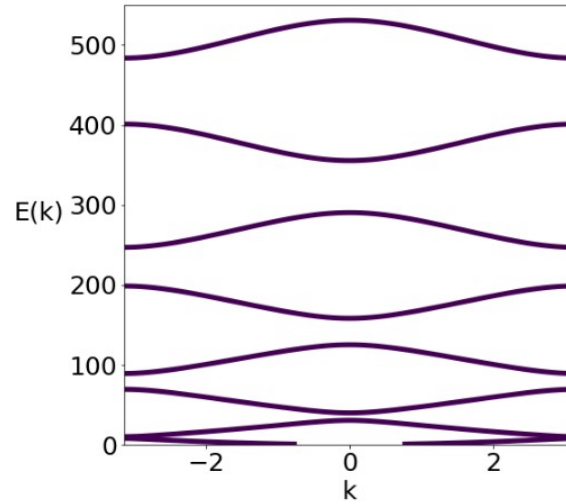


**Figure 4.** Graph of the transcendental energy equation of the triangular potential for  $w = 1000$ ,  $b = 0.001$ ,  $a = 1$ , and the area  $A = bw = 1$ . The missing points appear in the domain of the wave number  $k \in [-0.75, 0.75]$ .

In turn, Equation (24) can also be applied for asymmetric potentials, that is that  $V_1(x)$  is a portion of a rectangle or a triangle and  $V_2(x)$  is a portion of a triangle or a rectangle (Figure S1 in the Supplementary Materials), both of which have a known solution. The energy functions  $N_1(E), N_2(E), N_3(E)$ , and  $N_4(E)$  and their corresponding simulation of the transcendental energy equation (Figure S2 in the Supplementary Materials) are shown in detail in Section S3 of the Supplementary Materials of this paper.

### 3.3. The Group Speed

The group speed equation was already calculated in the theoretical part of this paper, and it is given by Equation (35). Therefore, below, we analyze the cases of known one-dimensional periodic potentials. Group speed values are shown in Tables S1–S3 in Section S6 of the Supplementary Materials of this paper.

#### 3.3.1. Dirac Delta Potential

The energy derivatives of the functions  $f(E)$  and  $g(E)$  to calculate the  $H_0(E)$  of Equation (36) are as follows:

$$f(E) = \frac{P\hbar}{\sqrt{2mEa}} \tag{48}$$

$$g(E) = 1, \tag{49}$$

$$\frac{df(E)}{dE} = -\frac{P\hbar m}{a(2mE)^{3/2}} \tag{50}$$

$$\frac{dg(E)}{dE} = 0. \tag{51}$$

For the group speed, the variable  $H_0(E)$  for the Dirac delta potential is obtained by substituting Equations (48)–(51) into Equation (36). The result of  $H_0(E)$  is given by the following equation:

$$H_0(E) = \left( \frac{am}{\hbar\sqrt{2mE}} + \frac{P\hbar m}{a(2mE)^{3/2}} \right) \sin \left( \frac{\sqrt{2mE}a}{\hbar} \right) - \left( \frac{P}{2E} \right) \cos \left( \frac{\sqrt{2mE}a}{\hbar} \right). \quad (52)$$

In Figure 5, one can see that, as the  $P$  value of the Dirac delta potential decreases, the maximum of the group speed increases.

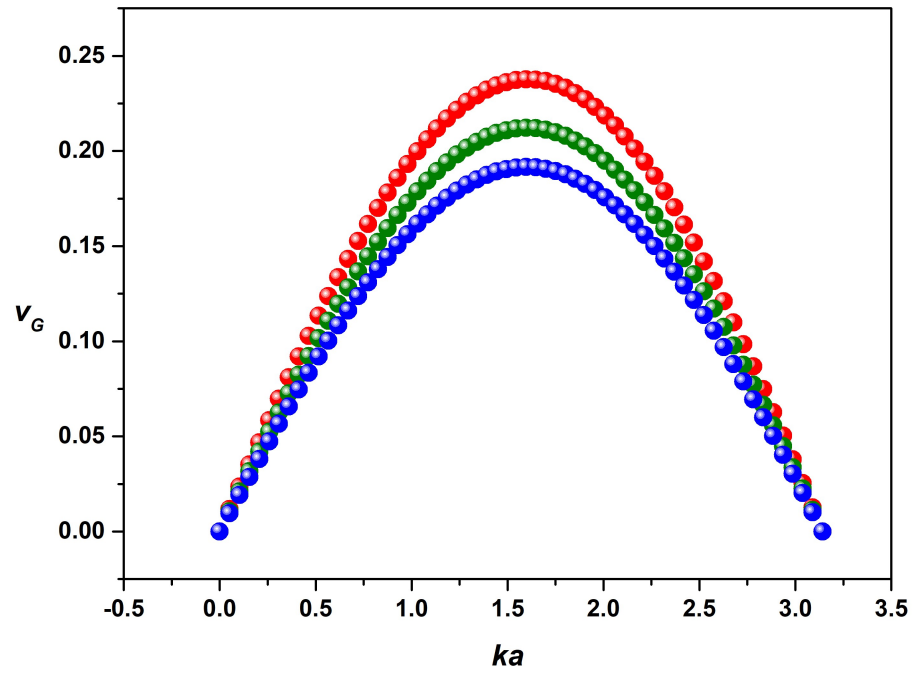


**Figure 5.** Group speed for different  $P$  values. Red color corresponds to  $P = 80$ , green color to  $P = 90$ , and blue color to  $P = 100$ . The separation  $a$  between the delta potentials is equal to 1. The graph shows the simulation of the group speed for the Dirac delta potential for 60 energy values, after substituting Equation (52) into Equation (35).

### 3.3.2. Rectangular Potential

The energy derivatives of the functions  $f(E)$  and  $g(E)$  to calculate the  $H_0(E)$  (36) are on this occasion much more extensive, since  $g(E)$  is not a constant:

$$f(E) = \left( \frac{w - 2E}{2\sqrt{E(w - E)}} \right) \sinh \left( \frac{2\sqrt{2m(w - E)}b}{\hbar} \right), \quad (53)$$

$$g(E) = \cosh \left( \frac{2\sqrt{2m(w - E)}b}{\hbar} \right), \quad (54)$$

$$\frac{df(E)}{dE} = -\frac{w^2}{4(E(w - E))^{3/2}} \sinh \left( \frac{2\sqrt{2m(w - E)}b}{\hbar} \right) - \frac{bm(w - 2E)}{\hbar\sqrt{2mE}(w - E)} \cosh \left( \frac{2\sqrt{2m(w - E)}b}{\hbar} \right), \quad (55)$$

$$\frac{dg(E)}{dE} = -\frac{2bm}{\hbar\sqrt{2m(w - E)}} \sinh \left( \frac{2\sqrt{2m(w - E)}b}{\hbar} \right). \quad (56)$$

For the group speed, the variable  $H_0(E)$  for the rectangular potential is obtained by substituting Equations (53)–(56) into Equation (36). The result of  $H_0(E)$  reads:

$$\begin{aligned}
 H_0(E) = & \frac{ma}{\hbar\sqrt{2mE}} \cosh\left(\frac{2\sqrt{2m(w-E)}b}{\hbar}\right) \sin\left(\frac{\sqrt{2mE}}{\hbar}\right) \\
 & + \frac{w^2}{4(E(w-E))^{3/2}} \sinh\left(\frac{2\sqrt{2m(w-E)}b}{\hbar}\right) \sin\left(\frac{\sqrt{2mE}}{\hbar}\right) \\
 & + \frac{\sqrt{m}b(w-2E)}{\hbar\sqrt{2E}(w-E)} \cosh\left(\frac{2\sqrt{2m(w-E)}b}{\hbar}\right) \sin\left(\frac{\sqrt{2mE}}{\hbar}\right) \\
 & + \frac{a\sqrt{m}(w-2E)}{2E\hbar\sqrt{2(w-E)}} \sinh\left(\frac{2\sqrt{2m(w-E)}b}{\hbar}\right) \cos\left(\frac{\sqrt{2mE}}{\hbar}\right) \\
 & - \frac{\sqrt{2m}}{\hbar\sqrt{w-E}} \sinh\left(\frac{2\sqrt{2m(w-E)}b}{\hbar}\right) \cos\left(\frac{\sqrt{2mE}}{\hbar}\right).
 \end{aligned} \tag{57}$$

Figure 5 shows that, as the value of  $P$  of the potential barrier decreases, the maximum group speed increases. However, as shown in Figure 6, the width of the rectangular potential also plays a major role, as the group speed varies greatly for different widths of the rectangle potential at a fixed height  $w = 100$ .

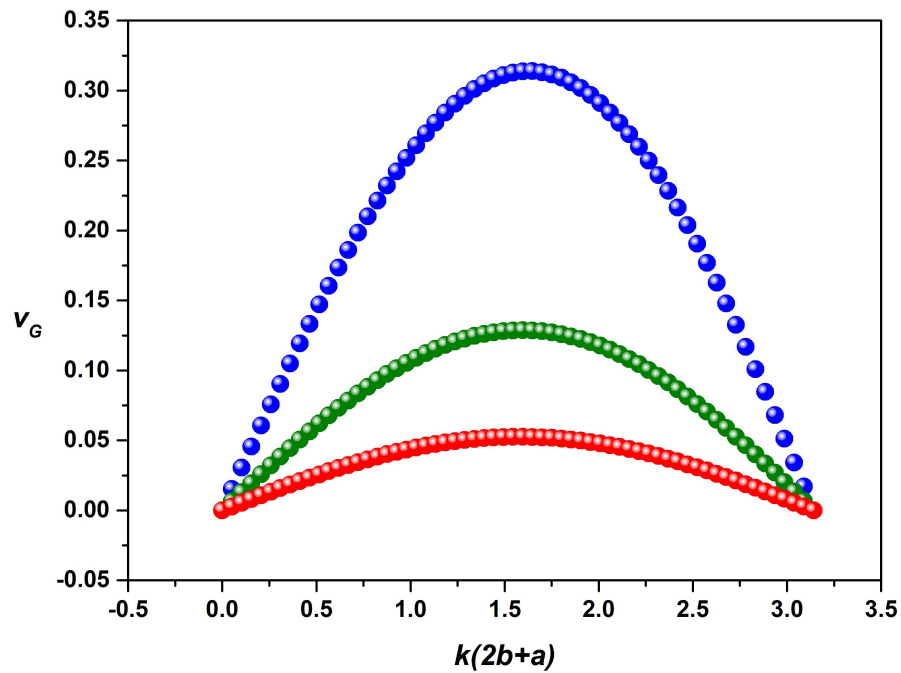


**Figure 6.** Group speed for different values of the width of the rectangle. Red color corresponds to  $b = 0.15$ , green color to  $b = 0.2$ , and blue color to  $b = 0.25$ . The separation  $a$  between the potentials is equal to 1. The simulation was carried out numerically with 60 energy values for the group speed in the rectangular potential, after substituting Equation (57) into Equation (35).

### 3.4. Effective Mass

Equation (39) is the analogous equation for the effective mass, which was determined similarly to the group speed. Only the graphs are included because the equations are very long, the corresponding equations are given in Section S5 of the Supplementary Materials of this paper. Effective mass values are given in Tables S1–S3 in Section S6 of the Supplementary Materials of this paper.

### 3.4.1. Dirac Delta Potential

Figure 7 depicts the effective mass discontinuity at a matching wave number. For different  $P$  values, the critical wave numbers and discontinuity energy are shown in Section S6 of the Supplemental Materials of this paper.

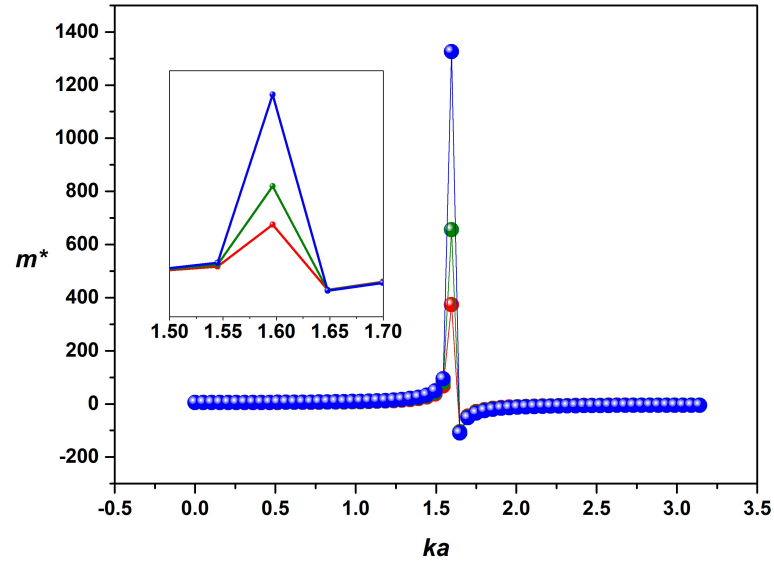


**Figure 7.** Effective mass for different  $P$  values. Red color corresponds to  $P = 80$ , green color to  $P = 90$ , and blue color to  $P = 100$ . The separation  $a$  between the potentials is equal to 1. Sixty energy values were used to numerically simulate the effective mass of the Dirac delta potential (39) derived in this paper.

### 3.4.2. Rectangular Potential

The discontinuity of the effective mass at a corresponding wave number can be seen in Figure 8. Furthermore, it is found that the width of the rectangular potential barrier has an effect on the effective mass.

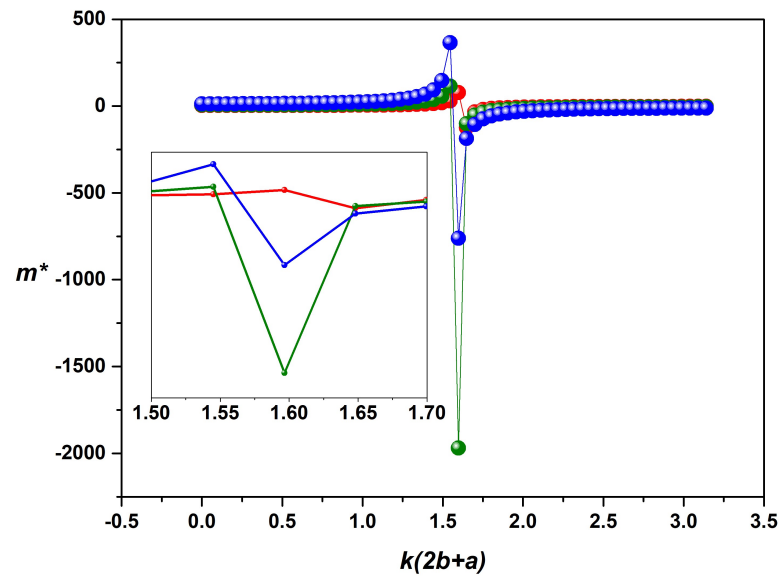


**Figure 8.** Effective mass for different values of the width of the rectangle. Red color corresponds to  $b = 0.15$ , green color to  $b = 0.2$ , and blue color to  $b = 0.25$ . Sixty energy values were used to numerically simulate the effective mass for the rectangular potential (39). The height  $w$  of the rectangle is equal to 100, and the space separation is  $a = 1$ .

For periodic potentials, the negative effective mass is referred to as holes, whereas the positive effective mass is referred to as electrons [30,31].

#### 4. Discussion

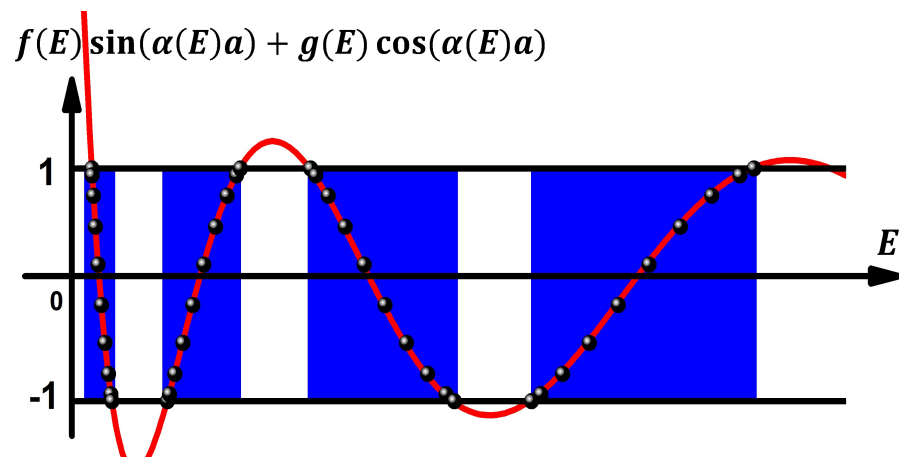
Using the equations for the periodic potential suggested in this study, suitable findings for the potentials known as the positive Dirac delta potential of positive intensity and rectangular potential were found. A transcendental energy equation for potentials other than the triangular potential could also be obtained. The transcendental energy equation was subsequently calculated for asymmetric potentials such the triangular–rectangular and rectangular–triangular potentials, which also approximate the Dirac delta potential.

Figure 9 depicts the periodic potential’s energy bands. The range of permitted and prohibited energies is likewise regarded:

$$-1 \leq \frac{\sin(\alpha a)}{\alpha} \left[ \frac{M_1(E) + \alpha^2 M_2(E)}{M_4(E)} \right] + \cos(\alpha a) \left[ \frac{M_3(E)}{M_4(E)} \right] \leq 1, \tag{58}$$

$$-1 \leq \frac{\sin(\alpha a)}{\alpha} \left[ \frac{N_1(E) + \alpha^2 N_2(E)}{N_4(E)} \right] + \cos(\alpha a) \left[ \frac{N_3(E)}{N_4(E)} \right] \leq 1. \tag{59}$$

Also, the energy values (black dots in Figure 9) that are solutions of the transcendental energy equation in the range of  $[-1, 1]$  are shown.



**Figure 9.** The energy dependence for the transcendental energy equation obtained in this paper; see Equation (31). The blue rectangles represent the energy bands.

Regarding group speed and effective mass, it was observed that the Dirac delta potential and the rectangular potential both have a predetermined shape in the first allowed energy band. Also, it was demonstrated that both potentials are canceled out at the extremes of group speed. This is to be expected given that these values indicate the boundaries of permissible and prohibited energy bands in the periodic potential. The change in group speed orientation for the second energy band is depicted in Figure 10.

Unlike the first energy band, where the group speed is positive, the group speed in the second energy band is negative and has a higher value. This is visible for both of the analyzed potentials (Dirac delta and rectangular).

The orientation of the group speed will depend on the shape of the proper transcendental energy equation curve. This is written as a function of the derivative of the energy with the wave number as in Equation (34). If the rate of change is positive then the group speed is positive; on the other hand, if the rate of change is negative, then the group speed will be negative [32]. This is observed in the first energy band in Figures 5 and 6 and for the second energy band in Figure 10 regarding the periodic Dirac delta and rectangular potentials.

These results must be valid for symmetric periodic potentials in which  $V_1(x) = V_2(x)$ . However, for asymmetric periodic potentials in which  $V_1(x) \neq V_2(x)$ , it is not possible to

ensure that this is totally true, since at least in the current study, it has only been verified for asymmetric potentials that can be simulated numerically.

It is also necessary to note that the results of the graphs obtained from the energy transcendental equation—the group speed and the effective mass—are in agreement with those reported in the literature [32,33]. The reason why the negative part of the domain of the wave number  $k$  was not simulated for the group speed and effective mass is because it is not truly necessary, since such wave number behavior can be deduced by means of even and odd functions, from the transcendental energy equation, which is an even function.

Figure 11A,C well demonstrates that the value of  $P$  of the Dirac delta function influences the change in the value of the wave number  $ka$  at which the effective mass discontinuity is observed, whereas Figure 11B,D show that the width of the rectangular potential also influences the value of the wave number  $k(2b+a)$  at which the effective mass discontinuity occurs.

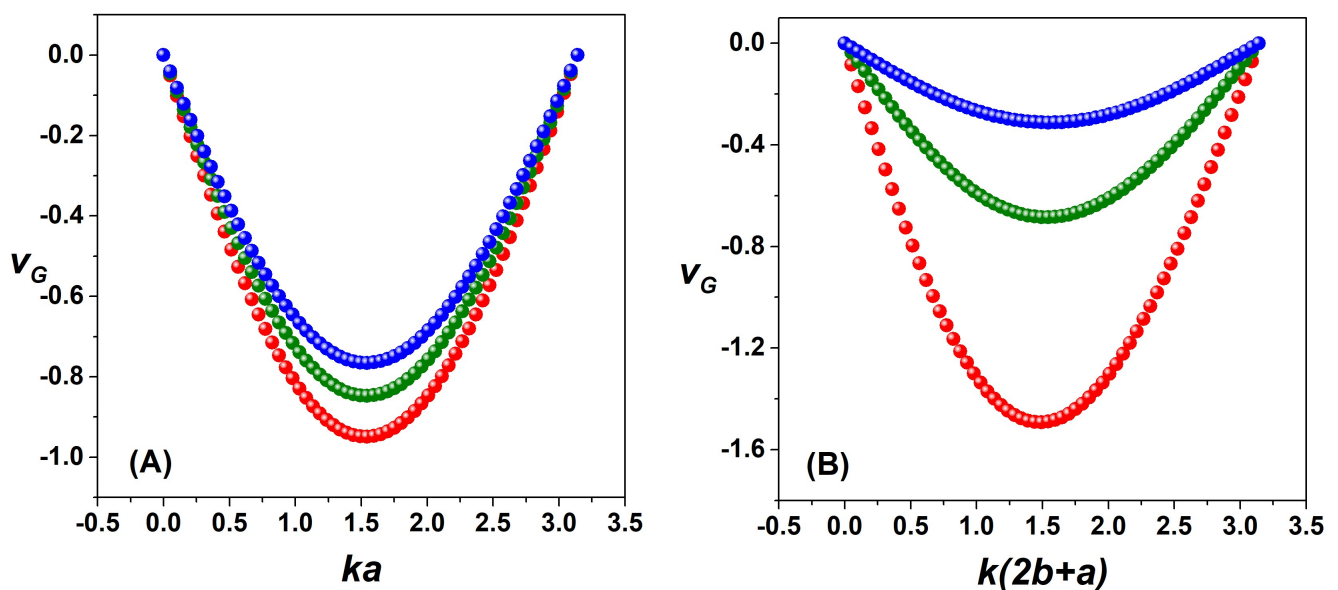


**Figure 10.** (A) Group speed for different  $P$  values of the potential barrier. Red color corresponds to  $P = 80$ , green color to  $P = 90$ , and blue color to  $P = 100$ . (B) Group speed for different values of the width of the rectangle. Red color for  $b = 0.15$ , green color for  $b = 0.2$ , and blue color for  $b = 0.25$ . The height of the potentials is  $w = 100$ . The separation between the potential barriers in (A,B) is the same and is  $a = 1$ .

In the case of effective mass, it was demonstrated that there is an energy-dependent discontinuity. This energy is also the transcendental energy equation's turning point, that is the energy at which the transcendental energy equation equals the change in concavity. The calculation of the discontinuity value  $k$  and the discontinuity energy using Equation (42) is a complicated task as soon as it requires knowing of at least one of these quantities, because the energy is an implicit function of the wave number, as noted in Equations (15) and (24).

Therefore, to calculate these variables, this was performed by means of the average between the maximum  $k$  and the minimum  $k$  of the effective mass, in the same way as for the case of energy, taking the average of the maximum  $E$  and the minimum  $E$  from the minimum  $k$  and maximum  $k$  obtained previously from the effective mass. All this procedure was performed using the high-level programming language Python.

One can see these results in the effective mass for the studied potentials (Dirac delta, rectangular). When the  $P$  values of Dirac delta potentials were changed, that value of the wave number in which it presented discontinuity changed, cf Figures 7 and 11C; in the same way, having changed the height of the rectangular potential, the value of the wave number that presents the discontinuity changes, cf Figures 8 and 11D. In turn, let us note

that the effective mass for both potentials in the second energy band shown in Figure 11A,B compared to Figures 7 and 8 does not show a change in the discontinuity of the effective mass. The height of the potentials is a constant equal to 100 in Figure 11. The separation between the potential barriers is equal to 1 in Figure 11.

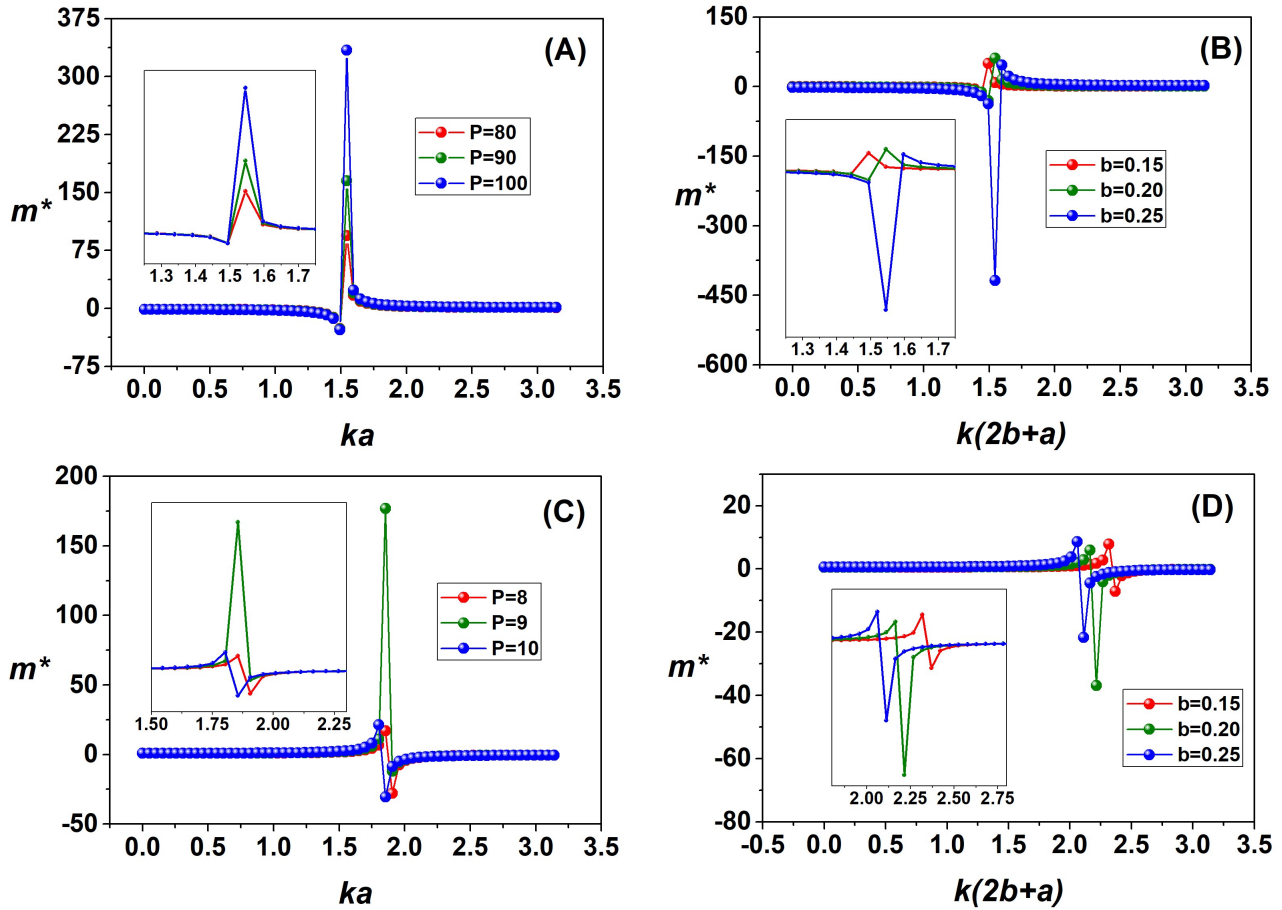


**Figure 11.** Effective mass in the first and second energy bands: (A) second energy band of the Dirac delta potential, (B) second energy band of the rectangular potential, (C) first energy band of the Dirac delta potential, and (D) first energy band of the rectangular potential.

In Section S6 of the Supplementary Materials to this paper, the values of  $k(2b + a)$  and of the energy  $E$  are presented, where the discontinuity occurs, both for the first and second energy bands for the Dirac delta and rectangular potentials. Although transcendental energy equations were obtained for the periodic triangular potential and its combinations with the rectangular potential, the equations of these potentials for the transcendental energy equation, the speed of the group, and the effective mass are quite lengthy, so not given here. However, it is possible to perform the numerical simulation of this potential, and the values of those quantities can be found in Sections S3–S5 of the Supplementary Materials of this paper.

Further on, for the periodic triangular potential, Figure 12A shows its group speed and Figure 12B shows its effective mass. It is worth noting that the shape of the group speed and effective mass did not change in relation to the other periodic potentials and, similarly, for the asymmetric periodic potentials presented in Figures S3 and S4 of the Supplementary Materials of this paper.

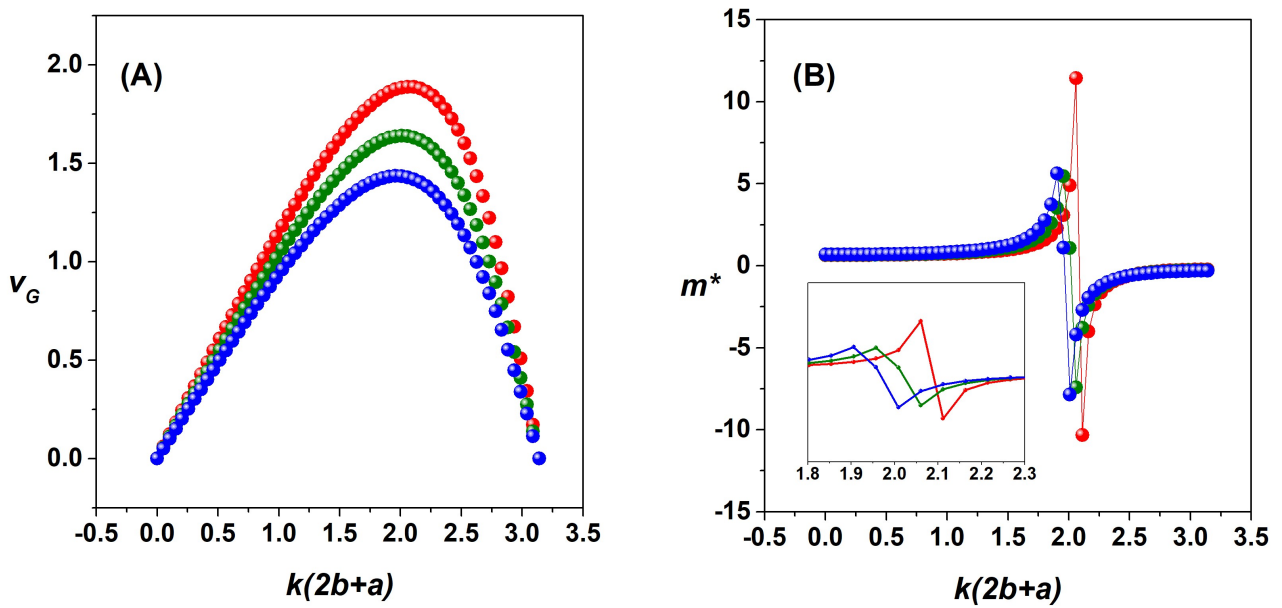


**Figure 12.** (A) Group speed for different values of the width of the triangle. Red color corresponds to  $b = 0.15$ , green color to  $b = 0.2$ , and blue color to  $b = 0.25$ . The height of the potentials is a constant equal to 10. (B) Effective mass for different values of the width of the triangle. Red color corresponds to the width  $b = 0.15$ , green color to  $b = 0.2$ , and blue color to  $b = 0.25$ . The height  $w$  of the potentials is a constant equal to 10. The separation  $a$  between the potential barriers in (A,B) is the same and equal to 1.

Comparing the three examined potentials, as shown in Figure 13, one makes quite differing observations. The group speed of the rectangular potential is larger than that of the triangular potential in Figure 13A, but the effective mass of the rectangular potential appears more shifted in Figure 13B.

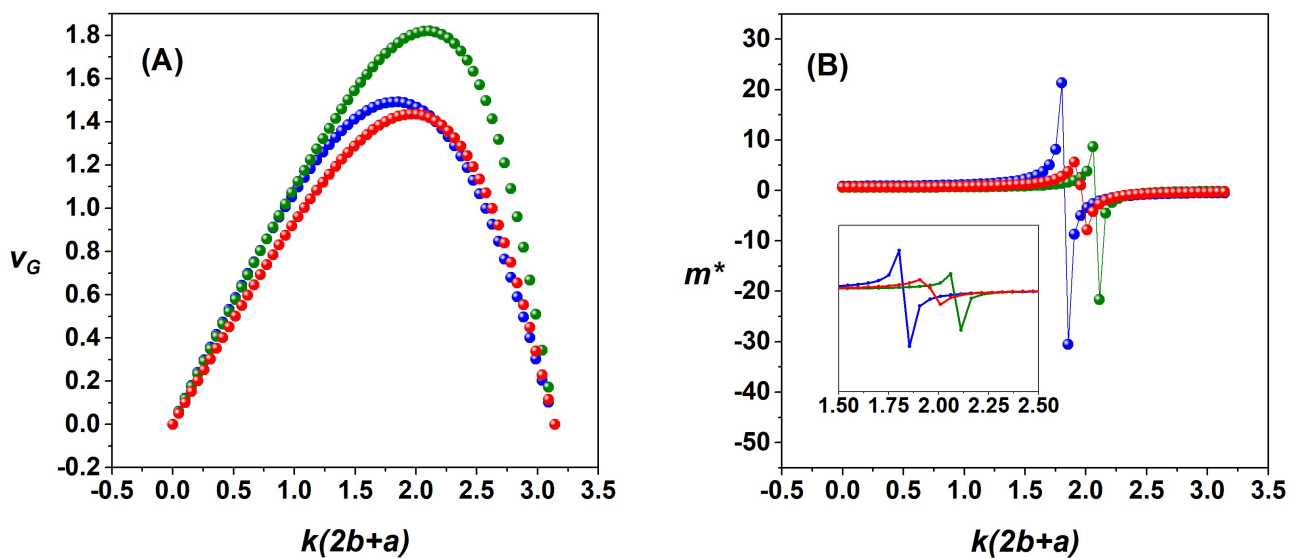


**Figure 13.** (A) Group speed for the three periodic potentials studied. Red color corresponds to triangular potential, green color to rectangular potential, and blue color to Dirac delta potential. (B) Effective mass for the three periodic potentials studied. Red color corresponds to triangular potential, green color to rectangular potential, and blue color to Dirac delta potential. The separation between the potential barriers in (A,B) is equal to 1; the width of the potentials is 0.25; the height of the potential barrier is constant and equal to 10.

## 5. Conclusions

In this paper, a transcendental energy equation was obtained for the periodic potentials of the form  $V = V(x)$ , the most-notable being the triangular, rectangular–triangular, and triangular–rectangular potentials. The equations obtained are shown in Equations (15) and (24). At the same time, the approximation to the Dirac delta periodic potential of positive intensity was also proposed through the corresponding limits for any type of periodic potential that has the form of Equation (1). From the obtained transcendental energy equation for the distinct periodic potentials, the group speed and the effective mass were calculated from Equations (35) and (39). The Dirac delta periodic potential was compared to these potentials based on the group speed and effective mass. The presented simulations agreed with the analytical expressions for both physical parameters. Finally, a future contribution for the work performed would be to develop an algorithm to calculate the transcendental energy equation, group speed, and effective mass for more-complex periodic potentials.

**Supplementary Materials:** The following supporting information can be downloaded at: <https://www.mdpi.com/article/10.3390/physics6010006/s1>. Section S1: Periodic potential of a potential ( $V = V(x)$ ) and a zero potential; Section S2: Periodic potential of two potentials  $V = V(x)$  and a zero potential; Section S3: The transcendental energy equation; Section S4: The group speed; Section S5: The effective mass; Section S6: Supplementary tables; Figure S1: Representation of asymmetric periodic potentials. (A) Rectangular-triangular periodic potential, (B) Triangular-rectangular periodic potential; Figure S2: Periodic asymmetric potential with separation between the asymmetric potentials  $a = 1$ ; width of the asymmetric potential  $b = 0.001$ , and height of the asymmetric potential  $w = 1000$ . (A) Periodic asymmetric rectangular–triangular potential. (B) Periodic asymmetric triangular–rectangular potential; Figure S3: Group speed with width  $b = 0.25$ ; spacing between potentials  $a = 1$ , and height  $w = 10$ . Blue color for the periodic potential asymmetrical rectangular–triangular, green color for the periodic triangular potential, and red color for the periodic potential asymmetrical triangular–rectangular; Figure S4: Effective mass with width  $b = 0.25$ ; spacing between potentials  $a = 1$ , and height  $w = 10$ . Blue color blue for the periodic potential asymmetrical rectangular–triangular, green color for the periodic triangular potential, and red color for the periodic potential asymmetrical triangular–rectangular; Table S1: Values of  $ka$ ,  $v_G$ , and  $E$  for the group speed and effective mass of the Dirac delta potential. The value of  $a = 1$ ; Table S2: Values of  $k(2b + a)$ ,  $v_G$ , and  $E$  for the group speed and effective mass of the rectangular potential. The values of  $a = 1$  and  $b = 0.001$ . ND = Not Defined; Table S3: Values of  $k(2b + a)$ ,  $v_G$ , and  $E$  for the group speed and effective mass of the triangular potential, triangular–rectangular potential, and rectangular–triangular potential in the first band energy. The values of  $a = 1$  and  $b = 0.001$ . ND = Not Defined.

**Author Contributions:** Conceptualization, F.M.-V. and R.M.E.-B.; methodology, F.M.-V. and R.M.E.-B.; software, F.M.-V.; validation, J.A.R.-G. and R.M.E.-B.; formal analysis, F.M.-V. and R.M.E.-B.; investigation, F.M.-V., J.A.R.-G. and R.M.E.-B.; resources, F.M.-V.; data curation, F.M.-V.; writing—original draft preparation, F.M.-V.; writing—review and editing, F.M.-V., J.A.R.-G. and R.M.E.-B.; visualization, F.M.-V., J.A.R.-G. and R.M.E.-B.; supervision, J.A.R.-G. and R.M.E.-B.; project administration, F.M.-V. and R.M.E.-B.; funding acquisition, R.M.E.-B. All authors have read and agreed to the published version of the manuscript.

**Funding:** We thank the Programa de Subvencion Financiera a Publicaciones de Investigadores UNMSM en Revistas Indizadas de Alto Impacto 2023 and to Vicerrectorado de Investigación y Posgrado (VRIP) de la Universidad Nacional Mayor de San Marcos (UNMSM), Peru, for financially supporting this work. The APC was covered by grant R.R. N.° 013566-2023-R/UNMSM and R.D. N° 01284-DGA-2023.

**Data Availability Statement:** The original data related to this research can be requested at any time by the first author's email: [freddy.mendoza1@unmsm.edu.pe](mailto:freddy.mendoza1@unmsm.edu.pe).

**Conflicts of Interest:** The authors declare no conflicts of interest.

## References

1. Singleton, J. *Band Theory and Electronic Properties of Solids*; Oxford University Press: Oxford, UK, 2001. [CrossRef]
2. Li, C.-L.; Xu, Y. Influence of time-periodic potentials on electronic transport in double-well structure. *Chin. Phys. B* **2010**, *19*, 057202. [CrossRef]
3. Solaimani, M. Binding energy and diamagnetic susceptibility of donor impurities in quantum dots with different geometries and potentials. *Mater. Sci. Eng. B* **2020**, *262*, 114694. [CrossRef]
4. Pavelich, R.L.; Marsiglio, F. The Kronig-Penney model extended to arbitrary potentials via numerical matrix mechanics. *Am. J. Phys.* **2015**, *83*, 773–781. [CrossRef]
5. Le Vot, F.; Meléndez, J.J.; Yuste, S.B. Numerical matrix method for quantum periodic potentials. *Am. J. Phys.* **2016**, *84*, 426–433. [CrossRef]
6. You, S.K.; Jeon, K.J.; Kim, C.K.; Nahm, K. A new approximation scheme in quantum mechanics. *Eur. J. Phys.* **1998**, *19*, 179–186. [CrossRef]
7. Carrillo, R.S.; Gil-Barrera, C.A.; Sun, G.-H.; Solaimani, M.; Dong, S.-H. Shannon entropies of asymmetric multiple quantum well systems with a constant total length. *Eur. Phys. J. Plus* **2021**, *136*, 1060. [CrossRef]
8. Carrillo, R.S.; Dong, Q.; Sun, G.-H.; Silva-Ortigoza, R.; Dong, S.-H. Shannon entropy of asymmetric rectangular multiple well with unequal width barrier. *Results Phys.* **2022**, *33*, 105109. [CrossRef]
9. Chen, C.-Y.; Wang, X.-H.; You, Y.; Sun, G.-H.; Dong, S.-H. Exact solutions of the rigid rotor in the electric field. *Int. J. Quantum Chem.* **2020**, *120*, e26336. [CrossRef]
10. Chen, C.-Y.; You, Y.; Wang, X.-H.; Lu, F.-L.; Sun, D.-S.; Dong, S.-H. Exact solutions of the angular Teukolsky equation for particular cases. *Results Phys.* **2021**, *24*, 104–115. [CrossRef]
11. Chen, C.-Y.; Lu, F.-L.; Sun, G.-H.; Wang, X.-H.; You, Y.; Sun, D.-S.; Dong, S.-H. Exact solution of rigid planar rotor in external electric field. *Results Phys.* **2022**, *34*, 105330. [CrossRef]
12. Dong, S.-H.; Dong, S.; Dong, Q.; Sun, G.-H.; Femmam, S. Exact solutions of the Razavy cosine type potential. *Adv. High Energy Phys.* **2018**, *2018*, 5824271. [CrossRef]
13. Sun, G.-H.; Chen, C.-Y.; Taud, H.; Yáñez-Márquez, C.; Dong, S.-H. Exact solutions of the 1D Schrödinger equation with the Mathieu potential. *Phys. Lett. A* **2020**, *384*, 126489. [CrossRef]
14. Chen, C.-Y.; Wang, X.-H.; You, Y.; Sun, D.-S.; Lu, F.-L.; Dong, S.-H. Exact solutions to the angular Teukolsky equation with  $s \neq 0$ . *Commun. Theor. Phys.* **2022**, *74*, 115001. [CrossRef]
15. Szmulowicz, F. Kronig-Penney model: A new solution. *Eur. J. Phys.* **1997**, *18*, 392. [CrossRef]
16. Behera, S.N.; Gayen, S.; Prasad, G.R.; Bose, S.M. Electronic properties of ordered and disordered linear clusters of atoms and molecules. *Phys. Condens. Matter* **2007**, *390*, 124–133. [CrossRef]
17. Vidal, V.E. Gas de Bosones en una Serie Finita de Capas Delgadas Penetrables. Ph.D. Thesis, Universidad Nacional Autónoma de México, Mexico City, Mexico, 2012. Available online: <https://hdl.handle.net/20.500.14330/TES01000695282> (accessed on 25 November 2023).
18. Gil, A.; Segura, J.; Temme, N.M. Numerical evaluation of Airy-type integrals arising in uniform asymptotic analysis. *J. Comput. Appl. Math.* **2020**, *371*, 112717. [CrossRef]
19. Nesvizhevsky, V.V.; Protasov, K.V. Quantum states of neutrons in the Earth's gravitational field: State of the art, applications, perspectives. In *Trends in Quantum Gravity Research*; Moore, D.C., Ed.; Nova Science Publishers, Inc.: Hauppauge, NY, USA, 2006; pp. 65–107. Available online: [https://www.researchgate.net/publication/252531650\\_Quantum\\_States\\_of\\_Neutrons\\_in\\_the\\_Earth%27s\\_Gravitational\\_Field\\_State\\_of\\_the\\_Art\\_Applications\\_and\\_Perspectives](https://www.researchgate.net/publication/252531650_Quantum_States_of_Neutrons_in_the_Earth%27s_Gravitational_Field_State_of_the_Art_Applications_and_Perspectives) (accessed on 25 November 2023).
20. Robinett, R.W. The Stark effect in linear potentials. *Eur. J. Phys.* **2009**, *31*, 1–14. [CrossRef]
21. Córdova, J.G.P.; Melo, E.R.; Walle, B.L. Estudio de los mecanismos de conducción eléctrica en películas delgadas de PVB. *Ingenierías* **2017**, *20*, 55–72. Available online: [https://www.researchgate.net/publication/340115738\\_Estudio\\_de\\_los\\_mecanismos\\_de\\_conduccion\\_electrica\\_en\\_películas\\_delgadas\\_de\\_PVB](https://www.researchgate.net/publication/340115738_Estudio_de_los_mecanismos_de_conduccion_electrica_en_películas_delgadas_de_PVB) (accessed on 25 November 2023).
22. Varela, J.M. Efecto túnel en semiconductores sometidos a campos eléctricos intensos. *Rev. Cient. Ing. Desarro.* **1999**, *5*, 27–32. Available online: <https://rcientificas.uninorte.edu.co/index.php/ingenieria/article/view/2207> (accessed on 25 November 2023).
23. Corona, G. Localización y Transporte en Medios Aleatorios en una y dos Dimensiones. Master's Thesis, Universidad Michoacana de San Nicolás de Hidalgo, Morelia, Mexico, 2017. Available online: [http://bibliotecavirtual.dgb.umich.mx:8083/xmlui/handle/DGB\\_UMICH/1232](http://bibliotecavirtual.dgb.umich.mx:8083/xmlui/handle/DGB_UMICH/1232) (accessed on 25 November 2023).
24. Grosso, G.; Parravicini, G.P. *Solid State Physics*; Academic Press/Elsevier Ltd.: Oxford, UK, 2014. [CrossRef]
25. Ashcroft, N.W.; Mermin, N.D. *Solid State Physics*; Harcourt College Publishers/Saunders College Publishing: Orlando, FL, USA, 1976. Available online: <https://archive.org/details/AshcroftSolidState> (accessed on 25 November 2023).
26. Zhang, L.W.; Liew, K.M. An element-free based solution for nonlinear Schrödinger equations using the ICVMLS-Ritz method. *Appl. Math. Comput.* **2014**, *249*, 333–345. [CrossRef]
27. Singh, S. Kronig-Penney model in reciprocal lattice space. *Am. J. Phys.* **1983**, *51*, 179. [CrossRef]
28. Busch, K.; von Freymann, G.; Linden, S.; Mingaleev, S.F.; Tkeshelashvili, L.; Wegener, M. Periodic nanostructures for photonics. *Phys. Rep.* **2007**, *444*, 101–202. [CrossRef]

29. Izquierdo Díaz, E.A. Funciones de Green Aplicadas a la Solución de Problemas de Contorno Basados en la Ecuación Diferencial de Airy. Ph.D. Thesis, Universidad de Nariño, San Juan de Pasto, Colombia, 2018. Available online: <http://sired.udenar.edu.co/5921/> (accessed on 25 November 2023).
30. González-Viñas, W.; Mancini, H.L. *Ciencia de los Materiales*; Editorial Ariel: Barcelona, Spain, 2003. Available online: <https://docplayer.es/52286780-Ciencia-de-los-materiales-wenceslao-gonzalez-vinas-hector-luis-mancini.html> (accessed on 25 November 2023).
31. Bloch, I. Ultracold quantum gases in optical lattices. *Nat. Phys.* **2005**, *1*, 23–30. [[CrossRef](#)]
32. Alvarez, L. Introduction of the concepts of hole and effective mass using an alternative to the  $E-k$  diagram. *Rev. Mex. Fis.* **2013**, *59*, 128–132. Available online: <https://www.scielo.org.mx/pdf/rmfe/v59n2/v59n2a5.pdf> (accessed on 25 November 2023).
33. Ó Náraigh, L.; O’Kiely, D. Homogenization theory for periodic potentials in the Schrödinger equation. *Eur. Phys. J.* **2012**, *34*, 19–32. [[CrossRef](#)]

**Disclaimer/Publisher’s Note:** The statements, opinions and data contained in all publications are solely those of the individual author(s) and contributor(s) and not of MDPI and/or the editor(s). MDPI and/or the editor(s) disclaim responsibility for any injury to people or property resulting from any ideas, methods, instructions or products referred to in the content.